Chapter 8

Control of a Looping Kite

In order to demonstrate the versatility of the proposed real-time iteration scheme we present here the control of an airborne kite as a periodic control example. The kite is held by two lines which allow to control the lateral angle of the kite, see Fig. 8.1. By pulling one line the kite will turn in the direction of the line being pulled. This allows an experienced kite pilot to fly loops or similar figures. The aim of our automatic control is to make the kite fly a figure that may be called a "lying eight", with a cycle time of 8 seconds (see Fig. 8.2). The corresponding orbit is not open-loop stable, so that feedback has to be applied during the flight – we will show simulation results where our proposed real-time iteration scheme was used to control the kite, with a sampling time of one second.

8.1 The Dual Line Kite Model

The movement of the kite at the sky can be modelled by Newton's laws of motion and a suitable model for the aerodynamic force. Most difficulty lies in the determination of suitable coordinate systems: we will first describe the kite's motion in polar coordinates, and secondly determine the direction of the aerodynamic forces.

8.1.1 Newton's Laws of Motion in Polar Coordinates

The position $p \in \mathbb{R}^3$ of the kite can be modelled in 3-dimensional Euclidean space, choosing the position of the kite pilot as the origin, and the third component p_3 to be the height of the kite above the ground. With m denoting the mass of the kite and $F \in \mathbb{R}^3$ the total force acting on the kite, Newton's law of motion reads

$$\ddot{p} = \frac{d^2 p}{dt^2} = \frac{F}{m}.$$

Let us introduce polar coordinates θ, ϕ, r:

$$p = \begin{pmatrix} p_1 \\ p_2 \\ p_3 \end{pmatrix} = \begin{pmatrix} r\sin(\theta)\cos(\phi) \\ r\sin(\theta)\sin(\phi) \\ r\cos(\theta) \end{pmatrix}.$$

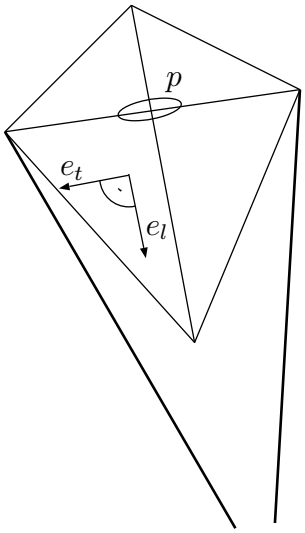

Figure 8.1: A picture of the kite.

Note that the distance r between pilot and kite is usually constant during flight, and θ is the angle that the lines form with the vertical. In these coordinates, $\ddot{p}$ looks as follows

$$\begin{aligned} \ddot{p} &= \frac{d}{dt}\left(\frac{\partial p}{\partial \theta}\dot{\theta} + \frac{\partial p}{\partial \phi}\dot{\phi} + \frac{\partial p}{\partial r}\dot{r}\right) \\ &= \frac{\partial p}{\partial \theta}\ddot{\theta} + \frac{\partial p}{\partial \phi}\ddot{\phi} + \frac{\partial p}{\partial r}\ddot{r} + \frac{\partial^2 p}{\partial \theta^2}\dot{\theta}^2 + \frac{\partial^2 p}{\partial \phi^2}\dot{\phi}^2 + \frac{\partial^2 p}{\partial r^2}\dot{r}^2 \\ &+ 2\frac{\partial^2 p}{\partial \phi \partial \theta}\dot{\phi}\dot{\theta} + 2\frac{\partial^2 p}{\partial r \partial \theta}\dot{r}\dot{\theta} + 2\frac{\partial^2 p}{\partial r \partial \phi}\dot{r}\dot{\phi}. \end{aligned} \tag{8.1}$$

Let us introduce a local right handed coordinate system with the three basis vectors

$$e_\theta = \begin{pmatrix} \cos(\theta)\cos(\phi) \\ \cos(\theta)\sin(\phi) \\ -\sin(\theta) \end{pmatrix}, \quad e_\phi = \begin{pmatrix} -\sin(\phi) \\ \cos(\phi) \\ 0 \end{pmatrix}, \quad \text{and} \quad e_r = \begin{pmatrix} \sin(\theta)\cos(\phi) \\ \sin(\theta)\sin(\phi) \\ \cos(\theta) \end{pmatrix}.$$

In this coordinate system, the partial derivatives of p with respect to θ, ϕ, r become

$$\frac{\partial p}{\partial \theta} = r e_\theta, \quad \frac{\partial p}{\partial \phi} = r\sin(\theta) e_\phi, \quad \text{and} \quad \frac{\partial p}{\partial r} = e_r,$$

and

$$\frac{\partial^2 p}{\partial \theta^2} = -r e_r, \quad \frac{\partial^2 p}{\partial \phi^2} = -r\sin^2(\theta) e_r - r\sin(\theta)\cos(\theta) e_\theta, \quad \text{and} \quad \frac{\partial^2 p}{\partial r^2} = 0,$$

as well as

$$\frac{\partial^2 p}{\partial \phi \partial \theta} = r\cos(\theta) e_\phi, \quad \frac{\partial^2 p}{\partial r \partial \theta} = e_\theta, \quad \text{and} \quad \frac{\partial^2 p}{\partial r \partial \phi} = \sin(\theta) e_\phi.$$

Eq. (8.1) can therefore be written as:

$$\begin{aligned}\ddot{p} &= e_\theta \left(r\ddot{\theta} - r\sin(\theta)\cos(\theta)\dot{\phi}^2 + 2\dot{r}\dot{\theta}\right) \\ &+ e_\phi \left(r\sin(\theta)\ddot{\phi} + 2r\cos(\phi)\dot{\phi}\dot{\theta} + 2\sin(\theta)\dot{r}\dot{\phi}\right) \\ &+ e_r \left(\ddot{r} - r\dot{\theta}^2 - r\sin^2(\theta)\dot{\phi}^2\right).\end{aligned}$$

Defining

$$F_\theta := F \cdot e_\theta, \quad F_\phi := F \cdot e_\phi, \quad \text{and} \quad F_r := F \cdot e_r,$$

we can write Newton's laws of motion in the form

$$\begin{aligned} r\ddot{\theta} - r\sin(\theta)\cos(\theta)\dot{\phi}^2 + 2\dot{r}\dot{\theta} &= \frac{F_\theta}{m}, \\ r\sin(\theta)\ddot{\phi} + 2r\cos(\theta)\dot{\phi}\dot{\theta} + 2\sin(\theta)\dot{r}\dot{\phi} &= \frac{F_\phi}{m}, \\ \ddot{r} - r\dot{\theta}^2 - r\sin^2(\theta)\dot{\phi}^2 &= \frac{F_r}{m}. \end{aligned} \tag{8.2}$$

If the length of the lines, denoted by r, is kept constant, all terms involving time derivatives of r will drop out. Furthermore, the last equation (8.2) will become redundant, as the force in the radial direction will be augmented by a constraint force contribution F_c, so that Eq. (8.2) is automatically satisfied when the augmented force $F_r' := F_r - F_c$ replaces F_r, with $F_c = F_r + r\dot{\theta}^2 + r\sin^2(\theta)\dot{\phi}^2$. In this case the equations of motion[1] simplify to

$$\ddot{\theta} = \frac{F_\theta}{rm} + \sin(\theta)\cos(\theta)\dot{\phi}^2, \tag{8.3}$$

$$\ddot{\phi} = \frac{F_\phi}{rm} - 2\cot(\theta)\dot{\phi}\dot{\theta}. \tag{8.4}$$

In our model, the force vector $F = F^{\text{gra}} + F^{\text{aer}}$ consists of two contributions, the gravitational force F^{gra} and the aerodynamic force F^{aer}. In cartesian coordinates, $F^{\text{gra}} = (0, 0, -mg)^T$ with $g = 9.81$ m s^{-2} being the earth's gravitational acceleration. In local coordinates we therefore have

$$F_\theta = F_\theta^{\text{gra}} + F_\theta^{\text{aer}} = \sin(\theta)mg + F_\theta^{\text{aer}} \quad \text{and} \quad F_\phi = F_\phi^{\text{aer}}.$$

It remains to derive an expression for the aerodynamic force F^{aer}.

8.1.2 Kite Orientation and the Aerodynamic Force

To model the aerodynamic force that is acting on the kite, we first assume that the kite's trailing edge is always pulled by the tail into the direction of the effective wind, as seen

[1] Note that the validity of these equations requires that $F_c = F_r + r\dot{\theta}^2 + r\sin^2(\theta)\dot{\phi}^2 \geq 0$, as a line can only pull, not push.

Name	Symbol	Value
line length	r	50 m
kite mass	m	1 kg
wind velocity	v_w	6 m/s
density of air	ρ	1.2 kg/m^3
characteristic area	A	0.5 m^2
lift coefficient	C_l	1.5
drag coefficient	C_d	0.29

Table 8.1: The kite parameters.

from the kite's inertial frame. Under this assumption the kite's longitudinal axis is always in line with the effective wind vector $w_e := w - \dot{p}$, where $w = (v_w, 0, 0)^T$ is the wind as seen from the earth system, and $\dot{p}$ the kite velocity. If we introduce a unit vector e_l pointing from the front towards the trailing edge of the kite (cf. Fig. 8.1), we therefore assume that

$$e_l = \frac{w_e}{\|w_e\|}.$$

The transversal axis of the kite can be described by a perpendicular unit vector e_t that is pointing from the left to the right wing tip. Clearly, it is orthogonal to the longitudinal axis, i.e.,

$$e_t \cdot e_l = \frac{e_t \cdot w_e}{\|w_e\|} = 0. \tag{8.5}$$

The orientation of the transversal axis e_t against the lines' axis (which is given by the vector e_r) can be influenced by the length difference Δl of the two lines. If the distance between the two lines' fixing points on the kite is d, then the vector from the left to the right fixing point is de_t, and the projection of this vector onto the lines' axis should equal Δl (being positive if the right wingtip is farther away from the pilot), i.e., $\Delta l = d\, e_t \cdot e_r$. Let us define the *lateral angle* ψ to be

$$\psi = \arcsin\left(\frac{\Delta l}{d}\right).$$

We will assume that we control this angle ψ directly. It determines the orientation of e_t which has to satisfy:

$$e_t \cdot e_r = \frac{\Delta l}{d} = \sin(\psi). \tag{8.6}$$

A third requirement that e_t should satisfy is that

$$(e_l \times e_t) \cdot e_r = \frac{w_e \times e_t}{\|w_e\|} \cdot e_r > 0, \tag{8.7}$$

which takes account of the fact that the kite is always in the same orientation with respect to the lines.

How to find a vector e_t that satisfies these requirements (8.5)–(8.7)? Using the projection w_e^p of the effective wind vector w_e onto the tangent plane spanned by e_θ and e_ϕ,

$$w_e^p := e_\theta(e_\theta \cdot w_e) + e_\phi(e_\phi \cdot w_e) = w_e - e_r(e_r \cdot w_e),$$

we can define the orthogonal unit vectors

$$e_w := \frac{w_e^p}{\|w_e^p\|} \quad \text{and} \quad e_o := e_r \times e_w,$$

so that (e_w, e_o, e_r) form an orthogonal right-handed coordinate basis. Note that in this basis the effective wind w_e has no component in e_o direction, as

$$w_e = \|w_e^p\| e_w + (w_e \cdot e_r) e_r.$$

We will show that the definition

$$e_t := e_w(-\cos(\psi)\sin(\eta)) + e_o(\cos(\psi)\cos(\eta)) + e_r \sin(\psi)$$

with

$$\eta := \arcsin\left(\frac{w_e \cdot e_r}{\|w_e^p\|}\tan(\psi)\right)$$

satisfies the requirements (8.5)–(8.7). Equation (8.5) can be verified by substitution of the definition of η into

$$e_t \cdot w_e = -\cos(\psi)\sin(\eta)\|w_e^p\| + \sin(\psi)(w_e \cdot e_r) = 0.$$

Eq. (8.6) is trivially satisfied, and Eq. (8.7) can be verified by calculation of

$$\begin{aligned}(w_e \times e_t) \cdot e_r &= (w_e \cdot e_w)\cos(\psi)\cos(\eta) - (w_e \cdot e_o)(-\cos(\psi)\sin(\eta)) \\ &= \|w_e^p\|\cos(\psi)\cos(\eta)\end{aligned}$$

(where we used the fact that $w_e \cdot e_o = 0$). For angles ψ and η in the range from $-\pi/2$ to $\pi/2$ this expression is always positive. The above considerations allow to determine the orientation of the kite depending on the control ψ and the effective wind w_e only. Note that the considerations would break down if the effective wind w_e would be equal to zero, or if

$$\left|\frac{w_e \cdot e_r}{w_e \cdot e_w}\tan(\psi)\right| > 1.$$

The two vectors $e_l \times e_t$ and e_l are the directions of aerodynamic lift and drag, respectively. To compute the magnitudes F_l and F_d of lift and drag we assume that the lift and drag coefficients C_l and C_d are constant, so that we have

$$F_l = \frac{1}{2}\rho\|w_e\|^2 A C_l \quad \text{and} \quad F_d = \frac{1}{2}\rho\|w_e\|^2 A C_d,$$

with ρ being the density of air, and A being the characteristic area of the kite.

Given the directions and magnitudes of lift and drag, we can compute F^{aer} as their sum, yielding

$$F^{\text{aer}} = F_l(e_l \times e_t) + F_d e_l$$

or, in the local coordinate system

$$F_\theta^{\text{aer}} = F_l((e_l \times e_t) \cdot e_\theta) + F_d(e_l \cdot e_\theta) \text{ and } F_\phi^{\text{aer}} = F_l((e_l \times e_t) \cdot e_\phi) + F_d(e_l \cdot e_\phi).$$

The system parameters that have been chosen for the simulation model are listed in Table 8.1. Defining the system state $x := (\theta, \dot{\theta}, \phi, \dot{\phi})^T$ and the control $u := \psi$ we can summarize the system equations (8.3)–(8.4) in the short form

$$\dot{x} = f(x, u),$$

with

$$f((\theta, \dot{\theta}, \phi, \dot{\phi})^T, \psi) := \begin{pmatrix} \dot{\theta} \\ \dfrac{F_\theta^{\text{aer}}(\theta, \dot{\theta}, \phi, \dot{\phi}, \psi)}{rm} + \sin(\theta)\dfrac{g}{r} + \sin(\theta)\cos(\theta)\dot{\phi}^2 \\ \dot{\phi} \\ \dfrac{F_\phi^{\text{aer}}(\theta, \dot{\theta}, \phi, \dot{\phi}, \psi)}{rm} - 2\cot(\theta)\dot{\phi}\dot{\theta} \end{pmatrix}.$$

8.2 A Periodic Orbit

Using the above system model, a periodic orbit was determined that can be characterized as a "lying eight" and which is depicted as a $\phi - \theta-$plot in Fig. 8.2, and as a time plot in Fig. 8.3. The wind is assumed to blow in the direction of the p_1-axis ($\theta = 90^o$ and $\phi = 0^o$). The periodic solution was computed using the off-line variant of MUSCOD-II, imposing periodicity conditions with period $T = 8$ seconds and suitable state bounds and a suitable objective function in order to yield a solution that was considered to be a meaningful reference orbit. Note that the control ψ (see Fig. 8.3) is positive when the kite shall turn in a clockwise direction, as seen from the pilot's viewpoint, and negative for an anti-clockwise direction. We will denote the periodic reference solution by $x_r(t)$ and $u_r(t)$. This solution is defined for all $t \in (-\infty, \infty)$ and satisfies the periodicity condition $x_r(t + T) = x_r(t)$ and $u_r(t + T) = u_r(t)$.

It is interesting to note that small errors accumulate very quickly so that the uncontrolled system will not stay in the periodic orbit very long during a numerical simulation (see Fig. 8.4). This observation can be confirmed by investigating the asymptotic stability properties of the periodic orbit.

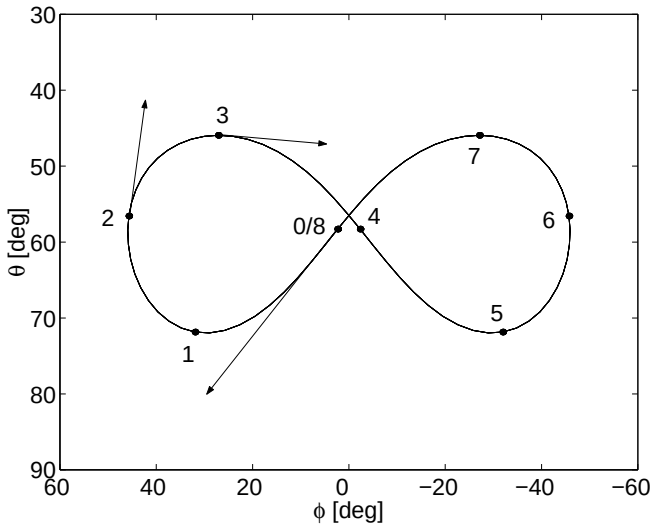

Figure 8.2: Periodic orbit plotted in the $\phi - \theta-$plane, as seen by the kite pilot. The dots separate intervals of one second.

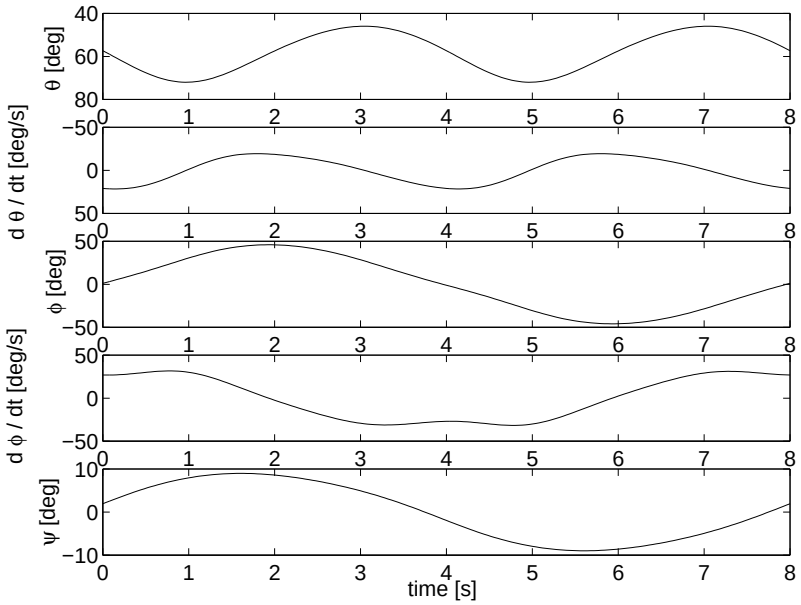

Figure 8.3: Periodic orbit: system states and control ψ plotted for one period $T = 8$ s . Note that θ and $\dot{\theta}$ oscillate with double frequency.

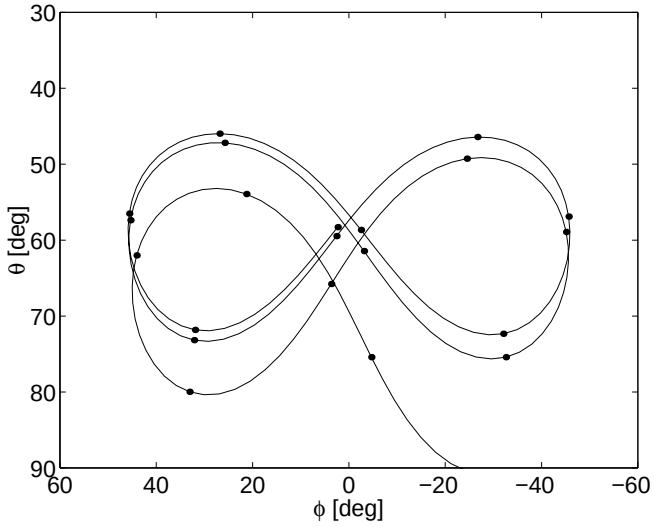

Figure 8.4: Open-loop control applied to the undisturbed system.

8.2.1 Stability Analysis of the Open-Loop System

To determine the asymptotic stability properties of the open-loop system along the periodic orbit, let us consider an initial value problem for the open-loop system on the interval $[0, T]$ corresponding to one period:

$$\begin{aligned} \dot{x}(t) &= f(x(t), u_r(t)), \quad \forall t \in [0, T], \\ x(0) &= x_0. \end{aligned}$$

The solution trajectories $x(t)$ can be regarded as functions of the initial value x_0. Note that for $x_0 = x_r(0)$ the solution is identical to the reference trajectory $x_r(t)$. The sensitivity matrices

$$W(t) := \frac{\partial x(t)}{\partial x_0}(x_r(0)), \quad t \in [0, T],$$

can therefore be obtained as the solution of the matrix initial value problem:

$$\begin{aligned} \dot{W}(t) &= \frac{\partial f}{\partial x}(x_r(t), u_r(t)) \cdot W(t) \quad \forall t \in [0, T], \\ W(0) &= \mathbb{I}_{n_x}. \end{aligned}$$

The final value $W(T)$ is called the *monodromy matrix*. It characterizes the sensitivity of the final state of each period with respect to the initial value. Asymptotically stable periodic orbits are characterized by a monodromy matrix whose eigenvalues (also called "Floquet Multipliers") all have a modulus smaller than one, which means that initial disturbances are damped out during the cycles. For a proof see e.g. Amann [Ama83].

A numerical computation of $W(T)$ for the kite model along the chosen periodic orbit yields

$$W(T) = \begin{pmatrix} 3.0182 & 2.4014 & 0.9587 & -0.1307 \\ 3.3399 & 2.5500 & 0.0054 & -0.3935 \\ -2.7170 & -1.8596 & 0.8436 & 0.5072 \\ -2.8961 & -2.0491 & 0.5601 & 0.4640 \end{pmatrix},$$

which has the eigenvalue spectrum

$$\sigma\left(W(T)\right) = \{\ 5.29, \quad 1.53, \quad 6.16 \cdot 10^{-2}, \quad 4.17 \cdot 10^{-7}\ \},$$

containing two eigenvalues that have a modulus bigger than one. This confirms that the system is asymptotically unstable in the periodic reference orbit.

8.3 The Optimal Control Problem

Given an initial state x_{t_0} at time t_0, an optimal control problem can be formulated that takes account of the objective to keep the system close to the reference orbit. For this aim we define a Lagrange term

$$L(x,u,t) := (x - x_r(t))^T Q (x - x_r(t)) + (u - u_r(t))^T R (u - u_r(t))$$

with diagonal weighting matrices

$$Q := \cdot \begin{pmatrix} 1.2 & 0 & 0 & 0 \\ 0 & 3.0\mathrm{s}^2 & 0 & 0 \\ 0 & 0 & 3.0 & 0 \\ 0 & 0 & 0 & 3.0\mathrm{s}^2 \end{pmatrix} 10^{-4}\mathrm{deg}^{-2}\mathrm{s}^{-1} \ \text{ and } \ R := 1.0 \cdot 10^{-2}\mathrm{deg}^{-2}\mathrm{s}^{-1}.$$

A hard constraint is given by the fact that we do not want the kite to crash onto the ground ($\theta = 90$ degrees), and for security, we require a path constraint function

$$h(x,u) := \left(75\,\mathrm{deg} - \theta\right)$$

to be positive. Using these definitions, we formulate the following optimal control problem on the moving horizon $[t_0, t_0 + 2T]$:

$$\begin{aligned} &\min_{u(\cdot),x(\cdot)} \int_{t_0}^{t_0+2T} L(x(t),u(t),t)\,dt && (8.8)\\ &\text{subject to} \\ &\qquad \dot{x}(t) = f(x(t),u(t)), && \forall t \in [t_0, t_0+2T], \\ &\qquad x(t_0) = x_{t_0}, \\ &h(x(t),u(t)) \geq 0, && \forall t \in [t_0, t_0+2T]. \end{aligned}$$

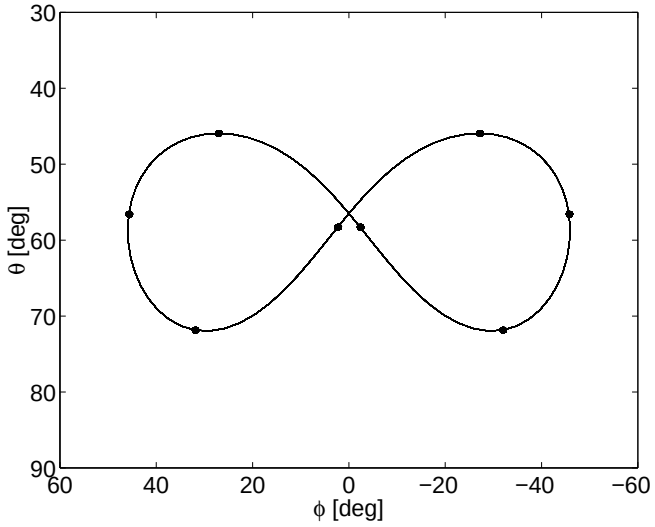

Figure 8.5: Closed-loop control applied to the undisturbed system, simulation of 100 periods. Numerical errors are attenuated by very small control responses (with $u(t) - u_r(t)$ in the order of 10^{-2} degree) and do not accumulate.

8.4 Closed-Loop Simulations

In the multiple shooting discretization the multiple shooting intervals were chosen to be each of one second length, thus allowing eight control corrections per period T. The Hessian matrix was approximated using the Gauss-Newton approach for integral least squares terms described in Sec. 6.4. The initialization of subsequent optimization problems was achieved with a shift strategy where the new final interval was initialized by an integration using the nominal open-loop control $u_r(t)$, cf. Sec. 4.4.1.

As a first test of the algorithm we try to control the undisturbed system, and the result of a simulation of 100 periods is depicted in Fig. 8.5. It can be seen that the reference orbit is perfectly tracked. The dots separate intervals of one second length and correspond to the sampling times.

For a second test we give the kite a slight "kick" at time $t = 1.0$ seconds that leads to a disturbance in the angular velocity $\dot{\theta}$. It changes from -1 deg/s to $+5$ deg/s. The closed-loop response is depicted in Fig. 8.6 as a $\phi - \theta-$plot.

As a third test we give the kite a moderate "kick" at time $t = 3.5$ seconds that lets the angular velocity $\dot{\theta}$ change from 12 deg/s to 25 deg/s. The closed-loop response is depicted in Fig. 8.7. For a comparison we also show the open-loop response to this disturbance in Fig. 8.8, which results in a crash 5 seconds after the disturbance.

In a fourth test we "kick" the kite strongly at time $t = 4.0$ seconds so that the angular velocity $\dot{\theta}$ changes abruptly from 20 deg/s to -7 deg/s. The closed-loop response is depicted in Fig. 8.9.

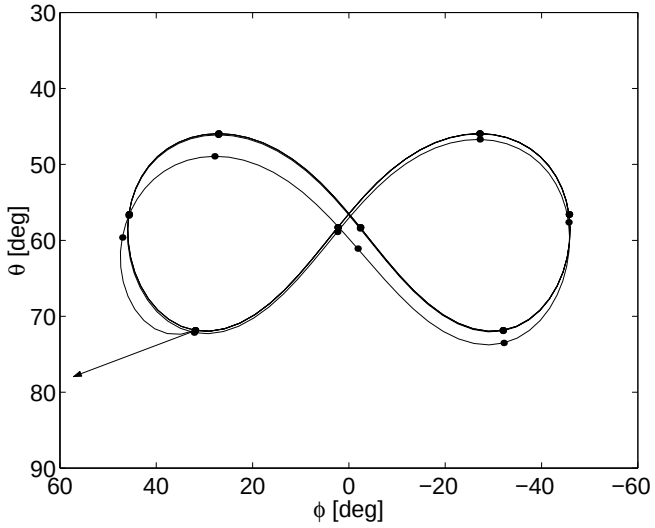

Figure 8.6: Closed-loop response to a small disturbance in $\dot{\theta}$ that changes from -1 deg/s to $+5$ deg/s at time $t = 1.0$ seconds. After one period the disturbance is nearly attenuated.

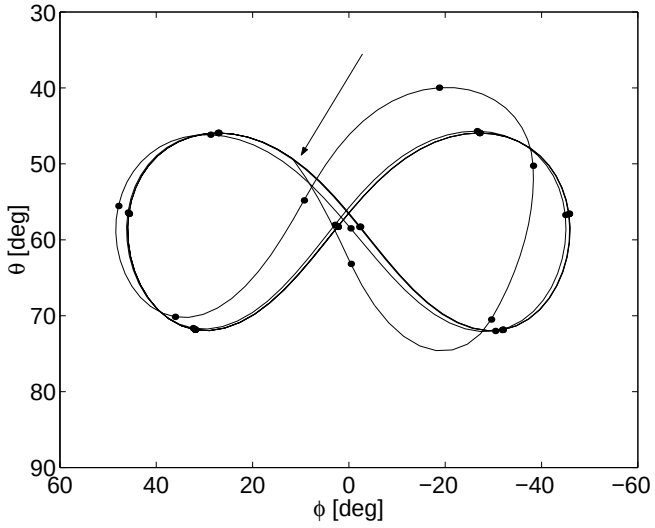

Figure 8.7: Closed-loop control response to a moderate disturbance in $\dot{\theta}$ that changes from 12 deg/s to 25 deg/s at time $t = 3.5$ seconds. After 1.5 periods the disturbance is attenuated.

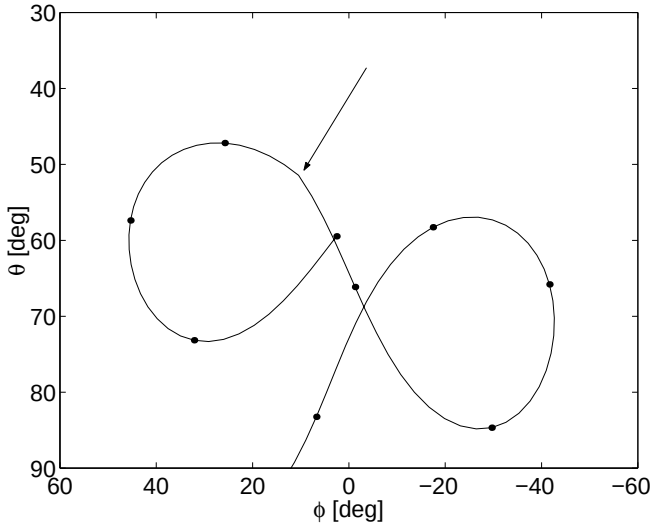

Figure 8.8: Open-loop response to the same disturbance as in Fig. 8.7, at time $t = 3.5$ seconds. Five seconds after the disturbance the kite crashes onto the ground (θ=90 degrees).

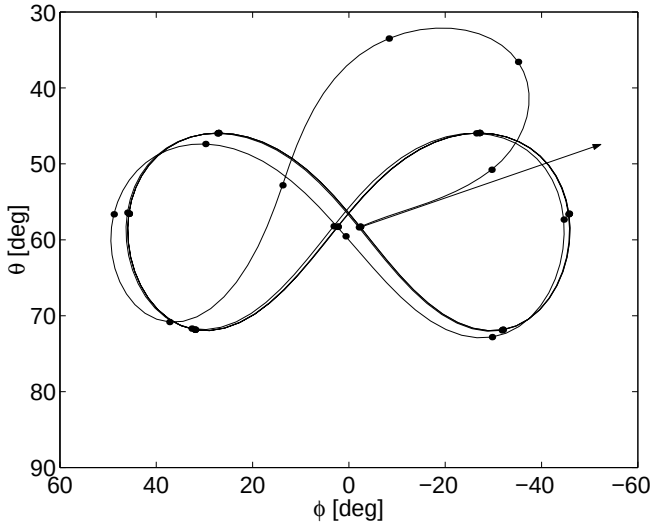

Figure 8.9: Closed-loop response to a strong disturbance in $\dot{\theta}$ that changes from 20 deg/s to a value of -7 deg/s at time $t = 4.0$ seconds. After two periods the disturbance is completely attenuated.

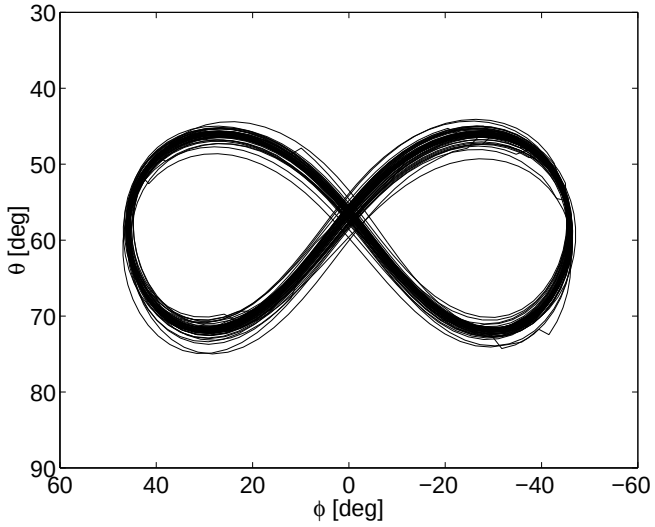

Figure 8.10: Closed-loop trajectory for the weak disturbance test, simulated over 100 periods.

As a last test we apply random noise of various magnitude to the system: disturbances happen with probability $p = 10\%$ s^{-1}, and they simultaneously disturb all 4 components of the system state, with independent magnitudes that are characterized by the standard deviations

$$s_\theta = 0.9\,\text{deg}, \quad s_{\dot\theta} = 0.9\,\text{deg s}^{-1}, \quad s_\phi = 0.6\,\text{deg}, \quad \text{and} \quad s_{\dot\phi} = 0.6\,\text{deg s}^{-1}$$

for the weak disturbance test, and

$$s_\theta = 4.5\,\text{deg}, \quad s_{\dot\theta} = 4.5\,\text{deg s}^{-1}, \quad s_\phi = 3\,\text{deg}, \quad \text{and} \quad s_{\dot\phi} = 3\,\text{deg s}^{-1}$$

for the strong disturbance test. For each scenario, we have carried out simulations for 100 periods (i.e., for 800 seconds). The resulting $\phi - \theta-$plots can be seen in Fig. 8.10 for the weak disturbance scenario, and in Fig. 8.11 for the strong disturbance scenario. While the weak scenario shows how nicely the closed-loop system behaves even in the presence of moderate disturbances, the strong disturbance scenario is certainly at the limits of the applicability of the chosen control approach, as the disturbances sometimes push the system state out of the state bounds specified in the optimization problem ($\theta \leq 75$ degrees). The resulting infeasibility of the optimization problems was cushioned by the relaxation strategy of the QP solver. However, this does not give any guarantee for the working of our approach in the presence of severe disturbances. Instead, a scheme employing soft constraint formulations should be employed.

The computation time for each real-time iteratiion cycle did not exceed the sampling time of one second in all simulations and averaged to 0.45 seconds with a standard deviation

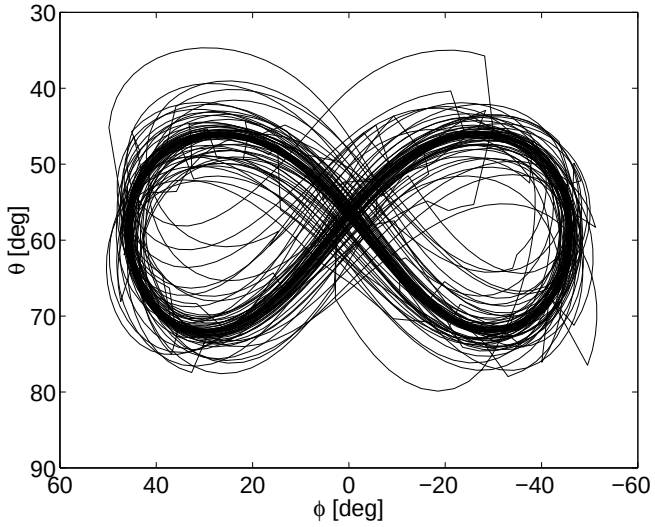

Figure 8.11: Closed-loop trajectory for the strong disturbance test, simulated over 100 periods.

of 0.02 seconds (on a Compaq Alpha XP1000 workstation). The immediate feedback took in average one tenth of this value, 0.05 seconds.